

Structural Basis of Eukaryotic Cell-Cell Fusion

Jimena Pérez-Vargas,^{1,2,8,9} Thomas Krey,^{1,2,8} Clari Valansi,³ Ori Avinoam,^{3,10} Ahmed Haouz,⁴ Marc Jamin,^{5,6,7} Hadas Raveh-Barak,³ Benjamin Podbilewicz,^{3,*} and Félix A. Rey^{1,2,*}

¹Institut Pasteur, Unité de Virologie Structurale, 25-28 Rue du Docteur Roux, 75724 Paris Cedex 15, France

²CNRS UMR 3569, 25-28 Rue du Docteur Roux, 75724 Paris Cedex 15, France

³Department of Biology, Technion—Israel Institute of Technology, Haifa 32000, Israel

⁴Institut Pasteur, Protéopôle—Plate-forme de Cristallogénèse, CNRS UMR 3528, 25-28 Rue du Docteur Roux, 75724 Paris Cedex 15, France

⁵Université Grenoble Alpes, 6 rue Jules Horowitz, UVHCI, 38042 Grenoble Cedex 9, France

⁶CNRS, UVHCI, 6 rue Jules Horowitz, 38042 Grenoble Cedex 9, France

⁷Unit for Virus Host-Cell Interactions, 6 rue Jules Horowitz, Université Grenoble Alpes-EMBL-CNRS, 38042 Grenoble Cedex 9, France

⁸Co-first author

⁹Present address: The Scripps Research Institute, 10550 North Torrey Pines Road, La Jolla, CA 92037, USA

¹⁰Present address: European Molecular Biology Laboratory, 69117 Heidelberg, Germany

*Correspondence: podbilew@technion.ac.il (B.P.), rey@pasteur.fr (F.A.R.)

<http://dx.doi.org/10.1016/j.cell.2014.02.020>

SUMMARY

Cell-cell fusion proteins are essential in development. Here we show that the *C. elegans* cell-cell fusion protein EFF-1 is structurally homologous to viral class II fusion proteins. The 2.6 Å crystal structure of the EFF-1 trimer displays the same 3D fold and quaternary conformation of postfusion class II viral fusion proteins, although it lacks a nonpolar “fusion loop,” indicating that it does not insert into the target membrane. EFF-1 was previously shown to be required in both cells for fusion, and we show that blocking EFF-1 trimerization blocks the fusion reaction. Together, these data suggest that whereas membrane fusion driven by viral proteins entails leveraging of a nonpolar loop, EFF-1-driven fusion of cells entails trans-trimerization such that trans-membrane segments anchored in the two opposing membranes are brought into contact at the tip of the EFF-1 trimer to then, analogous to SNARE-mediated vesicle fusion, zip the two membranes into one.

INTRODUCTION

Protein-driven membrane fusion events are essential in all forms of life. They are key to intracellular trafficking, neurotransmitter secretion, cell mating, and fertilization. They also play a crucial role in development of tissues and organs in multicellular organisms (Aguilar et al., 2013). Controlled membrane fusion relies on a thermodynamic coupling between a conformational change in fusion effector molecules—the so-called fusion proteins—and targeted membrane perturbations that lower the free energy barrier of an overall exothermic lipid merger reaction. Membrane fusion processes have been intensively studied in the case of intracellular fusion events (Wickner and Schekman, 2008), as

well as fusion of enveloped viral particles with a host cell during entry (Harrison, 2008; Kielian and Rey, 2006). These studies have shown that the fusion protein remains kinetically trapped in a metastable conformation—the “prefusion form”—until key interactions with the target membrane push it over the barrier to reach its lowest energy conformation, termed the “postfusion” form. The released energy is used to closely appose the two membranes together, while concomitantly destabilizing them at the site of fusion to drive lipid merger (Kozlov et al., 2010; Sapir et al., 2008).

Studies of intracellular fusion have revealed two families of fusion proteins, the “SNAREs”—acronym for “soluble N-ethylmaleimide-sensitive factor (NSF) attachment protein receptors” (Südhof and Rothman, 2009; Sutton et al., 1998)—and the dynamin-like “atlastin” GTPases (Bian et al., 2011; Byrnes and Sondernmann, 2011). In both cases, membrane merger results from trans-oligomerization of molecules anchored in the opposed membranes, followed by a conformational change that pulls the two membranes toward each other (Figure S1 available online; reviewed in Jahn and Scheller, 2006 and Moss et al., 2011).

In contrast to SNAREs and atlastins, viral fusion proteins do not trans-oligomerize in order to merge the two opposing membranes. Instead they bridge the two lipid bilayers via the formation of an extended intermediate that exposes a hydrophobic segment, termed fusion loop or fusion peptide, at the viral membrane distal end of the protein, such that it can insert into the target membrane (Figure S1B). The extended intermediate then collapses into a hairpin that brings together fusion loop and viral transmembrane (TM) segments, thereby forcing the two membranes into close apposition. Although the known viral fusion proteins belong to different structural “classes” based on their overall 3D fold, they all adopt a similar “hairpin” conformation in their final, postfusion form.

Extracellular cell-cell fusion processes are much less understood. An exception is placenta formation, where the envelope proteins of endogenous retroviruses mediate trophoblast fusion

through the same mechanism of virus-cell fusion reactions (Blond et al., 1999, 2000; Mi et al., 2000). The only genuine cellular fusion proteins were identified in *Caenorhabditis elegans* through genetic screens for a fusion failure phenotype (Mohler et al., 2002; Sapir et al., 2007). The identified proteins (PFAM14484) include epithelial fusion failure 1 (EFF-1) involved in hypodermis, vulva, and pharynx formation and anchor-cell fusion failure 1 (AFF-1), required for the formation of the hymen, pharyngeal muscles, and epidermal syncytia in nematodes. Amino acid sequence analyses have shown that EFF-1 and AFF-1 also have orthologs in other species, including arthropods, chordates, and protists (Avinoam et al., 2011; Avinoam and Podbilewicz, 2011). They are type I single TM proteins, with a bulky, glycosylated ectodomain displaying a conserved pattern of disulfide bonds and an unstructured cytosolic C-terminal tail. These common features led to the classification of these proteins within a broad fusion family (FF). Expression of EFF-1 or AFF-1 in *C. elegans* embryos induces fusion of cells in vivo (del Campo et al., 2005; Shemer et al., 2004). Also, syncytia formation is induced when they are ectopically expressed in cultured insect or mammalian cells (Avinoam et al., 2011; Podbilewicz et al., 2006; Sapir et al., 2007; Shilagardi et al., 2013). Importantly, fusion by EFF-1 or by AFF-1 was shown to require their presence in both cells to be fused (Podbilewicz et al., 2006; Sapir et al., 2007), suggesting a trans-oligomerization step to drive fusion (Sapir et al., 2008), similar to the mechanism described for the SNARE proteins (Figure S1A). It was also shown that rhabdovirus particles can be pseudotyped with AFF-1 replacing the authentic viral fusion glycoprotein at their surface (Avinoam et al., 2011). As expected, the pseudotyped particles required the presence of AFF-1 in the target cells in order to fuse, but they were also shown to fuse with cells expressing EFF-1 instead. This observation indicates that fusion can also occur in a heterotypic setting via AFF-1/EFF-1 interactions, suggesting that FF proteins are likely to share a common mechanism of action that is compatible with fusion activity across the family (Avinoam et al., 2011; Avinoam and Podbilewicz, 2011). Recently, EFF-1 was shown to require actin cytoskeletal rearrangements to drive fusion of cultured heterologous *Drosophila* cells. In these studies, EFF-1 was observed to cluster at the tip of actin-driven finger-like protrusions of the plasma membrane that invade neighboring cells (Shilagardi et al., 2013).

Here we show that recombinant expression of the EFF-1 ectodomain in *Drosophila* cells results in secretion of two forms, monomeric and trimeric, into the supernatant. We further report the crystal structure of the trimeric form to 2.6 Å resolution, revealing a striking homology to viral class II fusion proteins in their trimeric, postfusion hairpin conformation, although a hydrophilic segment replaces the fusion loop. We provide evidence that the monomeric form of EFF-1 is metastable and that trimerization is irreversible, matching the properties of the pre- and postfusion forms, respectively, of the viral counterparts (Bressanelli et al., 2004; Gibbons et al., 2004; Modis et al., 2004). We further show that blocking EFF-1 trimerization blocks membrane fusion and demonstrate additional functional parallels with viral class II fusion proteins, such as formation of an extended core trimer followed by folding back of the individual subunits into the postfusion hairpin conformation. In combina-

tion with available functional information, these results lead us to propose a trans-trimerization model for EFF-1-driven membrane fusion.

RESULTS AND DISCUSSION

Structure Determination

The production, crystallization, and structure determination of EFF-1 are reported in detail in the [Extended Experimental Procedures](#), and the statistics for diffraction data collection and for refinement of the atomic model are listed in [Table S1](#). In total, 461 amino acids out of 539 in the EFF-1 ectodomain (amino acids [aa] 23–561—i.e., the signal sequence is cleaved after residue 22) were traced in the experimental electron density map, from amino acids 34 to 560 (Figure 1) with internal breaks at loops 57–59, 80–100, 278–279, 393–396, and 510–545, which are disordered. We also crystallized a shorter version of the ectodomain, traced from aa 34–509, lacking the “stem” region (EFF-1_{Δstem}), which was instrumental in experimental phasing by real-space averaging of the electron density between different crystal forms.

Overall Organization of the EFF-1 Trimer

The atomic model shows that the EFF-1 protomer displays unambiguous structural homology to class II viral fusion proteins in their characteristic postfusion hairpin conformation (Figure 1A). The trimer subunits feature the three class II β sandwich domains, termed I, II, and III, organized in the same way as in the viral proteins (Figures 2 and S2) (Lescar et al., 2001; Rey et al., 1995). Four out of seven predicted N-linked glycosylation sites display electron density for the glycan chains, attached to residues N196 in domain II, N406 in the linker between domains I and III, and N428 and N467 in domain III (Figure 1). Structural comparisons using the Dali server (Holm and Park, 2000) resulted in Z scores ranging between 11 and 14 for about 320 Cα atoms of the viral counterparts (Table 1). A similar Z score is obtained when comparing flavivirus and alphavirus fusion proteins with each other. The EFF-1 Dali score is higher than that of the rubella virus (RV) counterpart (DuBois et al., 2013) when compared to the alphavirus or flavivirus proteins. Because RV belongs to the same family as the alphaviruses, this result indicates that EFF-1 has a 3D fold that is closer to that of “standard” class II proteins than does the fusion protein of a related virus.

The comparison with the viral class II protein trimers (Figure 2 and Table S2) unambiguously defines the membrane-facing side (top side in Figure 2A) and the membrane distal end (bottom side) of the EFF-1 trimer. In particular, domain III occupies the postfusion location observed in the viral proteins, a position it reaches only after the fusogenic reoligomerization process (Kielian and Rey, 2006). Multiple polar interactions, including 9 intra- and 18 interprotomer hydrogen bonds, stabilize domain III at the sides of the EFF-1 trimer (Table S3). The surface area buried by domain III is substantially more extensive in the contact with the neighbor subunit than in the intrasubunit contact (Figure 3A), indicating that the binding site for domain III becomes available only after formation of a “core” trimer of the domain I/II moieties interacting about the 3-fold molecular axis. This indicates that

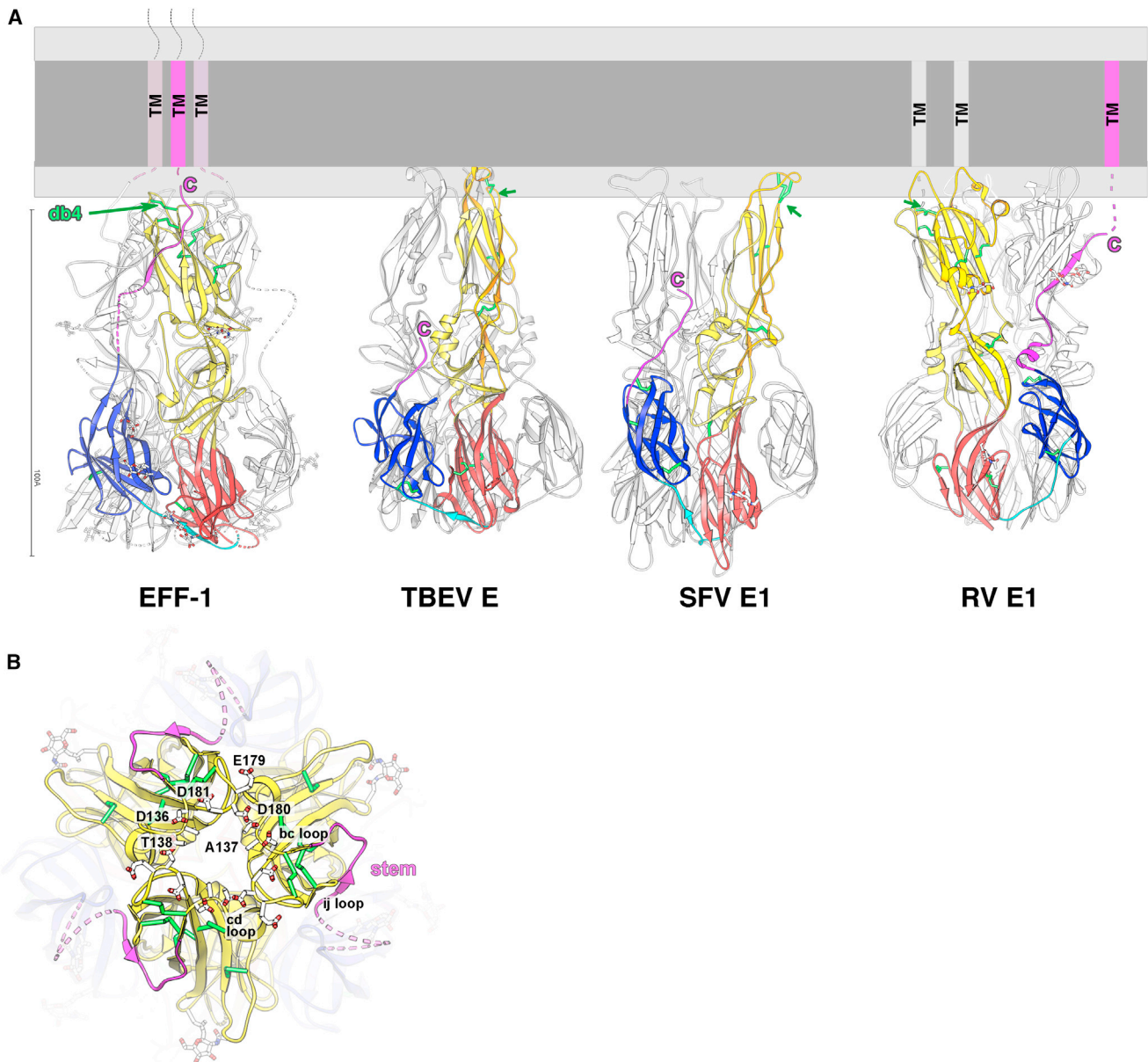


Figure 2. Comparison with Viral Class II Fusion Proteins

(A) Ribbon representation of the EFF-1 trimer shown next to the flavivirus (TBEV E, PDB 1URZ), alphavirus (SFV E1, PDB 1RER), and rubella virus (RV E1, PDB 4ADI) class II fusion protein trimers, with a scale bar (100 Å) on the left. A “fused” membrane is diagramed above, roughly to scale, with aliphatic and hydrophilic layers in dark and light gray, respectively. A reference subunit is shown in standard class II colors, and the others in gray, with disordered regions as dashed tubes; glycan chains and disulfide bonds are shown as in Figure 1. Green arrows point to the conserved class II protein disulfide bond (number 4 in Figure 1B). The inferred locations of the TM segments of EFF-1 and RV E1 are drawn following the MPR, to illustrate that they are brought into position to zipper across the membrane in EFF-1, whereas in RV E1, they would be too far from each other to interact within the membrane.

(B) Top view (as seen from the membrane, blown up from panel A) of the EFF-1 trimer showing side chains from residues of the *cd* loop and the top of the *bc* loop (labeled), together with the stem in magenta. The MPR of the stem converges toward the 3-fold molecular axis. See also Figure S3.

include the C-terminal part of the flavivirus stem, but we note an intriguing stretch of sequence similarity with EFF-1 (aa 549–553, highlighted in Figure 1B) near the membrane-proximal region (MPR), which suggests possible further structural similarities that may also have functional implications for understanding flavivirus fusion.

After the density break, the polypeptide chain “reemerges” (Figure S5) toward the tip of the trimer, at the level of the *ij* hairpin of domain II (Figures 1 and 3B). The broken lines in Figure 1A indicate the most straightforward, intrasubunit connection with domain III, although we cannot exclude a “strand-swapped” connection with an adjacent subunit in the trimer, as the

Table 1. Dali Scores Comparing the EFF-1 Ectodomain with Viral Class II Proteins

EFF-1	Alphavirus E1				Flavivirus E				RV E1 ^a										
	Z	N/N ^T	σ	I	Z	N/N ^T	σ	I	Z	N/N ^T	σ	I							
EFF-1	45.0	451/461	0.8	100	SFV	13.9	321/391	4.9	11	SLEV	12.7	333/386	5.8	9	RV	8.7	293/425	6.2	8
										TBEV	12.1	327/386	5.8	9					
										DEN1	12.2	320/379	5.8	10					
										DEN2	11.0	310/380	5.3	9					

For reference, Z scores below 2 are meaningless, whereas values of around 50 are obtained with the same protein. In this case, the score is between EFF-1 full ectodomain compared to EFF-1 truncated after domain III, which crystallize in different crystal forms and have different packing environments. “N/N^T” indicates the number of aligned residues (N) compared to the total residues in the alignment (N^T). σ is the root-mean-square deviation between C α atoms (in Å). “I” indicates % amino acid identity after the alignment. See also Table S2.

SFV, Semliki forest virus protein E1, PDB 1RER; SLEV, St. Louis encephalitis virus E protein, PDB 4FG0 (Luca et al., 2013); TBEV, tick-borne encephalitis virus protein E, PDB 1URZ; DEN“n,” dengue virus serotype “n” protein E (Modis et al., 2004; Nayak et al., 2009); RV, Rubella virus protein E1. ^aComparisons with RV E1e were performed with coordinates in which domain III was manually “unswapped” to make a trimer organized in the same way as EFF-1 or flavivirus E. Without this operation, the Dali score was based on fewer residues and the Z score value poorer.

disordered loop is long enough to span the distance. As discussed below, it appears more plausible that the connection is indeed intrasubunit (see section on EFF-1/AFF-1 heterotrimerization). The first six residues of the C-terminal stem region make β strand *n* (aa 546–551), which runs antiparallel to strand *j* as in the rubella virus E1 protein—the only class II molecule in which the stem is visible in the structure (DuBois et al., 2013). The MPR of the stem begins at residue 555 (after strand *n*), where the polypeptide chain crosses β sheets to run over the *bc* loop and end past the *cd* loop (Figures 3B and S5), stopping one residue short of the TM segment (aa 562–584). Although the last residue of the stem (D561) is disordered in the structure, its predicted location would add an additional carboxylate group facing the acidic patch discussed above, contributing to the negative electrostatic potential at the membrane-contacting side of the EFF-1 trimer. These carboxylates could form a divalent metal chelating site, which would contribute to further stabilizing the interaction of the stem with the body of the trimer. We were unable, however, to test the effect of adding divalent cations because of their insolubility in the presence of the high sulfate concentrations needed to grow diffraction-quality crystals of EFF-1 (see Extended Experimental Procedures).

The overall organization of the EFF-1 trimer, with a disordered 36 residue loop projecting out at the level of the central region of domain II (Figure 1A) and the polypeptide chain then joining the tip subdomain to converge toward the 3-fold axis at the membrane-facing end, is compatible with a putative interaction between TM segments in the final postfusion form. From their predicted locations in the structure, the TM segments can potentially zipper into a parallel three-helix bundle crossing the fused membrane (Figure 2A).

Monomeric EFF-1 Is Metastable

In order to further understand the EFF-1 fusogenic mechanism, it is worth considering similarities and differences in the modes of action of its viral counterparts. In the prefusion form, class II viral fusion proteins are maintained in a metastable array of dimers at the viral surface (Kuhn et al., 2002; Lescar et al., 2001). Dimer dissociation in the acidic environment of the endosome results in fusion-loop exposure and disassembly of the surface lattice.

A fusogenic conformational change of the fusion protein ensues, ending with the formation of stable postfusion homotrimers in which the protomer subunits are in a folded back, “hairpin” conformation with the fusion loops located next to the viral TM segments (Figure 2A). Although we have no information about the organization of EFF-1 in its prefusion form at the cell surface, we do obtain two distinct oligomeric forms of its ectodomain purified from the supernatant of the transfected *Drosophila* cells. This could be an indication that EFF-1 may also exist in a metastable (prefusion) form, which is subsequently triggered into a stable postfusion trimer. We therefore analyzed biochemically the recombinant ectodomain to see whether the two forms are in equilibrium with each other, or whether trimerization is irreversible. We observed that upon storage for several weeks at 0.1 mg/ml at 4°C, the monomer fraction gave back the two fractions, monomer and trimer, when reassayed by size exclusion chromatography (SEC). In contrast, the trimeric fraction did not give back monomers, even after dilution. Furthermore, concentration of the monomer fraction to ~10 mg/ml resulted in more than 80% conversion to trimer (Figures 4A and S6A), and back dilution to about 0.1 mg/ml did not yield back a monomer, confirming that EFF-1 trimerization is irreversible. These observations are thus compatible with metastable monomers being intermediates in a fusion process involving their irreversible conversion into postfusion trimers.

Structure-Guided Mutagenesis Aimed to Interfere with EFF-1 Trimerization

If trimer formation is essential for fusion, mutations affecting trimerization should be fusion impaired. Examining the crystal structure, we identified that residues G260, D321, and D322 are located at the interface such that mutations introducing longer side chains are likely to destabilize the EFF-1 trimer. We therefore prepared a G260A single, a D321E/D322E double, and G260A/D321E/D322E as well as G260E/D321E/D322E triple mutants. Analysis of the single- and double-mutant ectodomains by SEC showed less spontaneous trimerization than wild-type (WT), although they were still able to make trimers (Figure 4B). In contrast, the triple mutants, both of which behaved identically in our biochemical studies, showed almost

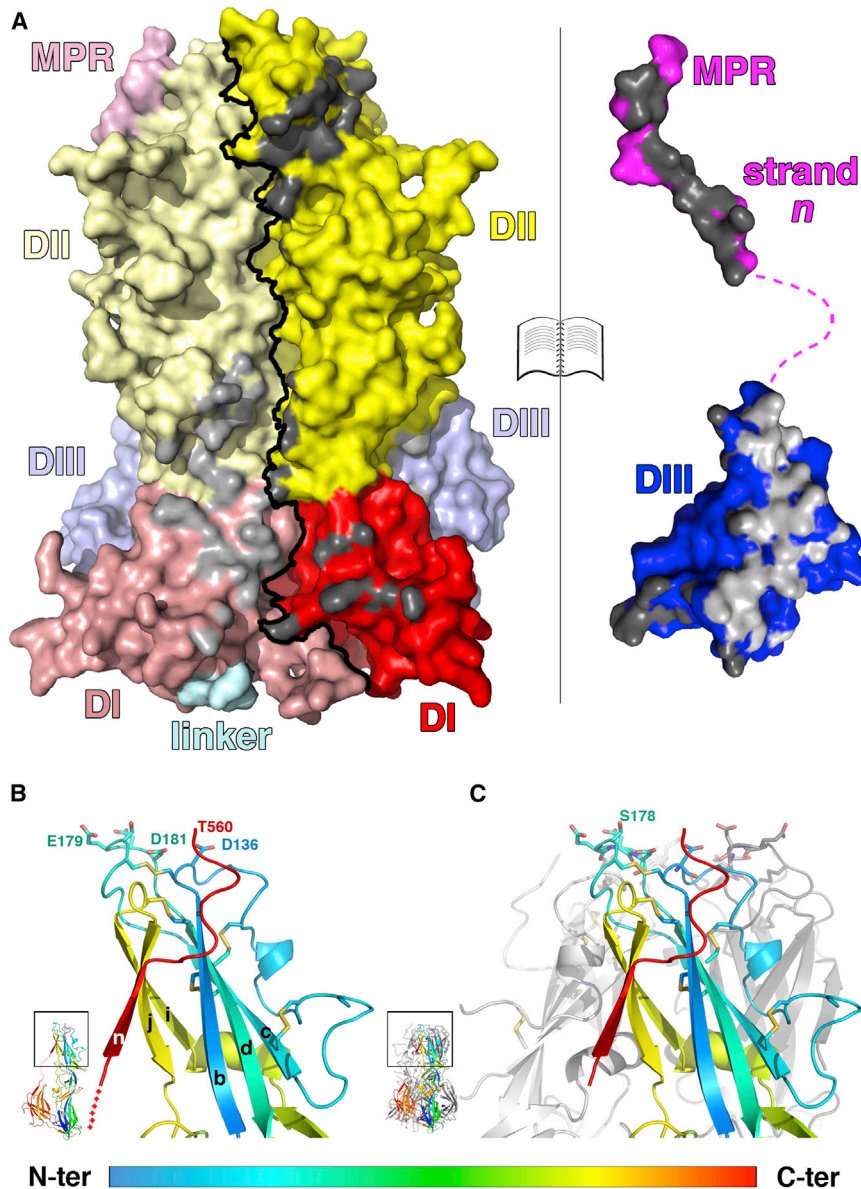


Figure 3. Interactions of Domain III and the Stem/MPR with the EFF-1 Core Trimer

(A) Contact area at the sides of the core trimer. The EFF-1 trimer is shown in surface representation and oriented as in Figure 2A, colored according to domains. Domain III and the stem from the reference subunit in front (highlighted in bright colors) were dissected out and placed in an “open book” orientation with respect to the body of the trimer. The adjacent protomers in the trimer (left panel) are in shaded colors to highlight intra- and interprotomer contacts made by domain III and the stem. The atoms in contact between the C-terminal segment (domain III and the stem) and the trimer core are colored dark and light gray for intra- and interprotomer interactions, respectively. The figure shows that the majority of the domain III contacts are interprotomeric, highlighting the trimer-stabilizing or “-clamping” role of domain III, whereas those from the stem are all intra-protomeric if the connectivity is that of Figure 1A. A thick black line follows the boundary in between subunits of the core trimer. See also Table S3. (B and C) Stem-domain II tip interactions. The EFF-1 subunit alone (B) and in the context of the trimer (C) are shown. The reference subunit was ramp-colored along the polypeptide chain as indicated by the bar underneath. Side chains of residues at the membrane interface, as well as disulfide bonds, are shown as sticks, with oxygen, nitrogen, and sulfur atoms red, blue, and yellow, respectively, and carbon atoms in the corresponding ramp color. Three distant segments of the polypeptide chain come together to form the tip: the *bdc* β sheet (residues 125–195, blue/cyan/pale green), the *ij* hairpin with the preceding short helix α B (residues 316–345, yellow), and the C-terminal end of the stem (residues 546–560, red), completing the antiparallel *nji* β sheet, which packs against *bdc* to form the tip β sandwich (strands labeled in B). The predicted location of D561, which is immediately before the TM segment, would be consistent with a chelation site for a divalent metal together with D181 and D136 (labeled in B). The box in the insets shows the location of the magnified area in each panel. See also Figure S5.

no trimerization under the conditions tested (Figure 4B, lower panel). The triple mutants nevertheless crystallized as trimers with the same postfusion conformation as WT, as shown by the 2.3 Å resolution structure of the G260A/D321E/D322E mutant, which displayed only a locally altered conformation of the polypeptide main chain to allow the packing of the A260 side chains about the 3-fold axis (Figure S6B). We did not pursue the analysis of the crystals of the G260E/D320E/D321E triple mutant because the diffraction pattern showed that they were isomorphous with the G260A/D321E/D322E crystals, indicating that both mutants have the same 3D structure. These results highlight an important plasticity of the EFF-1 trimerization interface, which appears tailored for a robust trimer interaction in spite of punctual changes at the contact surfaces.

Trimerization-Deficient EFF-1 Mutants Are Impaired in Cell Fusion

To test the cell fusion activity of the trimerization-defective mutants, we transiently expressed full-length mutant EFF-1 in BHK cells and analyzed protein localization and the extent of mutant EFF-1-driven multinucleation (Figure 4C, top panel). Analysis of multinucleation revealed that both mutant proteins tested (EFF-1 G260A and EFF-1 G260A/D321E/D322E) induced the formation of significantly less syncytia compared to WT (~20% compared to 46% for the mutants and WT EFF-1, respectively; Figure 4C). To determine whether the mutant proteins were expressed on the plasma membrane of BHK cells, we compared surface expression using cell-surface biotinylation (Figure 4C, lower panel) and indirect immunofluorescence (Figure S6C). We found that both mutants reached the cell surface

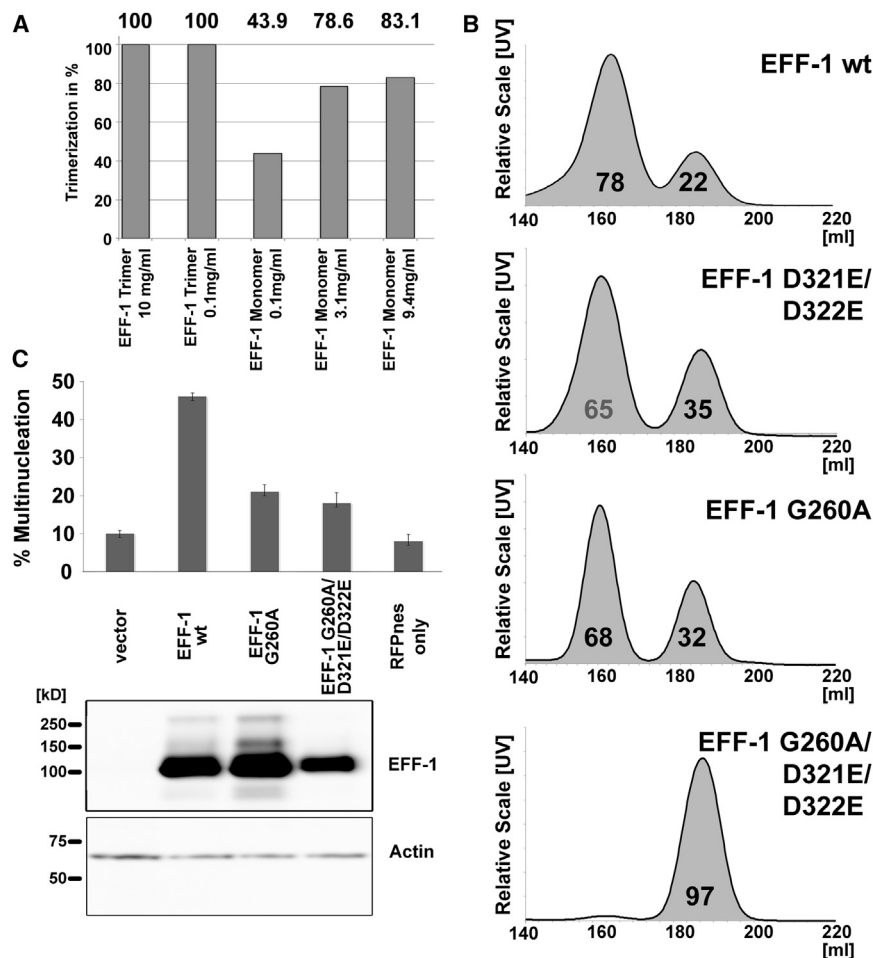


Figure 4. EFF-1 Trimerization Is Required for Cell-Cell Fusion

(A) Metastability of the WT EFF-1 monomeric ectodomain. The protein from each individual elution peak of an initial SEC run (as in the chromatograms shown in B) was concentrated or diluted to the indicated concentrations in the histogram and resampled by SEC. Each bar of the histogram displays the trimer/monomer ratios obtained in the second SEC run. The corresponding chromatograms are displayed in Figure S6A, along with the molecular masses of the two fractions determined by multiangle laser light scattering. See also Figure S6.

(B) Elution profiles from an Sdx200 size exclusion column obtained upon purification of soluble WT and mutant EFF-1 ectodomains from the supernatant of the *Drosophila* cell culture. The percentage of each form is calculated by peak integration and given in the shaded areas under the peaks. The top panel corresponds to a typical elution profile for WT protein. The ratio varied for different preparations, but the monomeric fraction was always around 20% ($\pm 5\%$) of the total WT protein, independent of the concentration of secreted protein in the supernatant. We did not make mutant preparations as many times as WT, but the chromatograms gave always above 30% monomer for the single and double mutants, indicating somewhat less propensity to form trimers. The triple mutant, in contrast, was almost 100% monomeric.

(C) The EFF-1 trimerization mutants are impaired in cell-cell fusion. Upper panel: multinucleation index for BHK cells expressing EFF-1 WT protein (46 ± 1 ; $n = 3522$), EFF-1 G260A mutant (21 ± 1.9 ; $n = 3207$), EFF-1 G260A/D321E/D322E mutant (18 ± 2.7 ; $n = 3396$), empty vector (10 ± 0.9 ; $n = 4058$), and RFPnes no vector ($8 \pm 1.9\%$; $n =$

3492). Results are mean of three independent experiments ($n \geq 1000$ for each experiment); $p < 0.005$ was calculated by two-tailed t test for both mutants compared to WT EFF-1. Data are presented as means \pm SEM. Lower panel: mutant and WT EFF-1 proteins carrying a V5 epitope fused to the cytoplasmic tail reach the cell surface in similar amounts. Surface biotinylation of transfected BHK cells was followed by affinity purification using neutravidin agarose beads and western blotting with an anti-V5 antibody (upper blot). No specific immunoreactivity is observed for the empty vector, whereas similar amounts of EFF-1 are detected for WT and both mutants sampled. A parallel western blot using the initial cell lysates and an anti-actin antibody served as loading control (lower blot).

at levels similar to those of WT, showing that they do not have a folding defect, and also that trimerization is not a requirement for reaching the cell surface. This is in line with the observation that their recombinant ectodomains are secreted at levels similar to those of WT and can be crystallized (Figure S6). These experiments provide a clear correlation between reduced trimerization of the EFF-1 mutant ectodomains and a significant reduction in syncytia formation induced by their full-length counterparts in cell culture, as would be expected if EFF-1 trimerization was required for EFF-1-driven cell-cell fusion. The similar reduction in multinucleation by the single and the triple mutants, in spite of the different trimerization abilities of their ectodomains, suggests that there may be a threshold in trimer stability that is important for fusion. An alternative explanation could be that the presence of the TM segments may partially compensate for the higher trimerization defect of the triple-mutant ectodomain. Taken together, these experiments indicate that formation of stable trimers is required to mediate cell-cell fusion.

Soluble EFF-1 Ectodomain Monomers Inhibit Syncytia Formation, whereas Trimers Do Not

To further test whether EFF-1 trimerization takes place during the fusion process, we tested the effect of adding soluble ectodomain to the supernatants of cells expressing the full-length, WT protein. For this purpose, we developed a stable cell line expressing an inducible construct of full-length EFF-1 to obtain a more uniform and mifepristone-regulated expression (see Extended Experimental Procedures). As shown in Figure 5A, addition of trimeric EFF-1-soluble ectodomain into the medium did not affect the amount of multinucleation of BHK cells following induction of full-length EFF-1. This observation is important because, were the fusion process to involve trimerization *in cis* and then trimer-trimer interactions across the two cells, the presence of soluble trimeric ectodomains would be expected to interfere with fusion. In contrast, addition of soluble monomeric EFF-1 had a clear inhibitory effect, as expected if fusion is driven by *in trans* interactions between prefusion

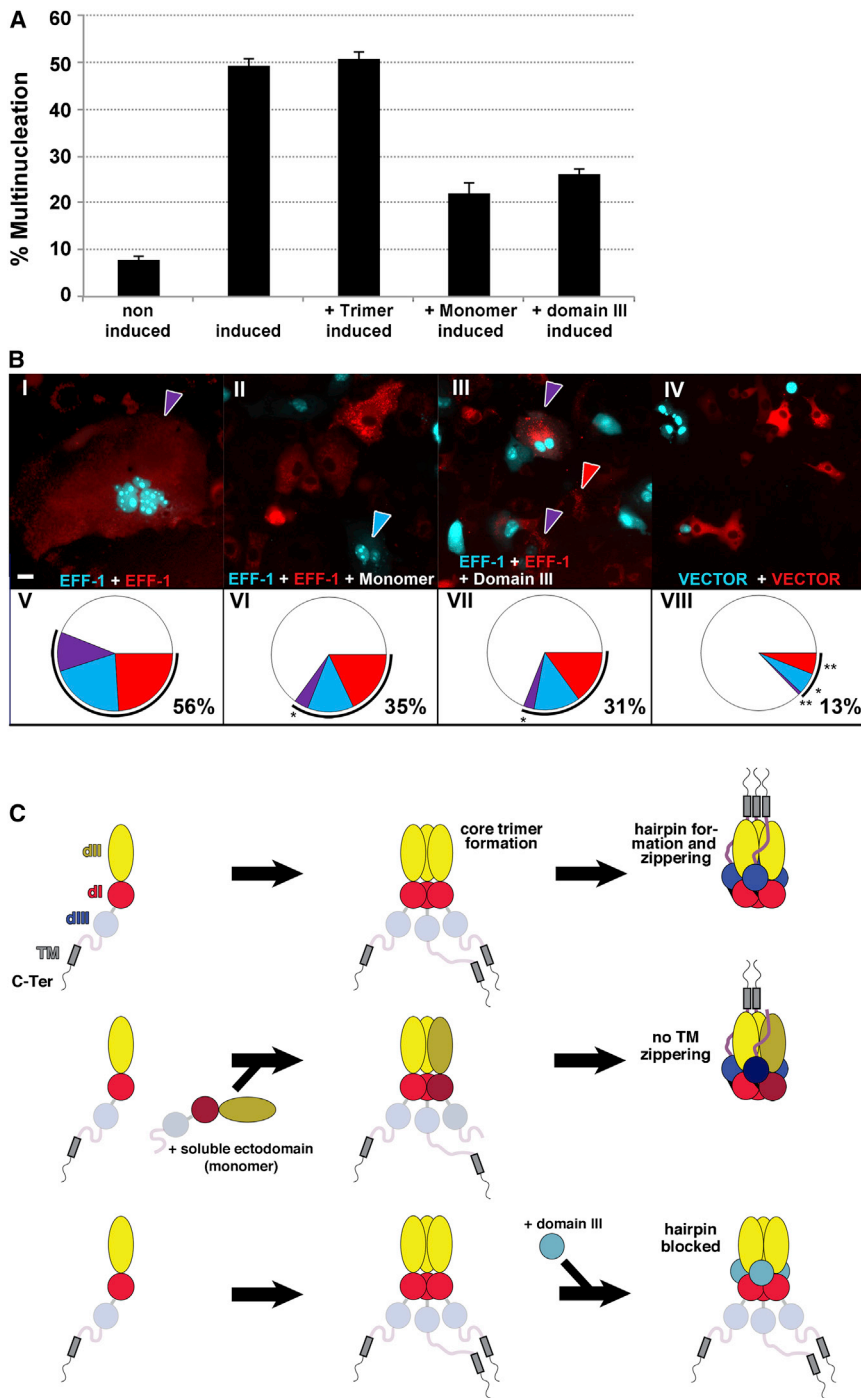


Figure 5. Monomeric EFF-1 Ectodomain or Soluble EFF-1 Domain III Inhibit EFF-1-Mediated Cell Fusion

(A) Multinucleation index for BHK cells expressing EFF-1 WT protein without (8 ± 0.8 ; $n = 500$) and with induction (49.2 ± 1.5 ; $n = 662$) and in the presence of recombinant EFF-1 trimeric ectodomain (50.8 ± 1.3 ; $n = 500$), EFF-1 monomeric ectodomain (22 ± 2.4 ; $n = 336$), and EFF-1 domain III (26 ± 1.2 ; $n = 525$). Data are presented as means \pm SEM. The lack of effect of the trimeric ectodomain, prepared exactly under the same conditions as the monomer, serves as an internal control for this experiment.

(B) Stable BHK cells transfected with an inducible EFF-1 full-length construct were further transfected with cytoplasmic RFP with a nuclear export signal (RFPnes) or nuclear CFP with a nuclear localization signal (CFPnl) and coincubated. (I) A multinucleated cell expressing CFP in the nuclei and RFP in the cytoplasm (purple arrowhead). Scale bar, 10 μ m. (II and III) The same experiment in the presence of 200 μ M EFF-1 monomeric ectodomain (II) or 200 μ M EFF-1 domain III (III). Binucleate cell, red and cyan arrowhead; mixed hybrid cells, purple arrowheads. (IV) Mixed BHK cells expressing empty vector transfected with RFPnes or CFPnl (control). (V–VIII) Quantification of cytosol mixing experiments. Red, cyan, and purple pie sections represent the percentage of multinucleation (two or more nuclei) for single-colored cells (red or cyan) and bicolored cells (purple). The remaining mononucleated cells are represented in white. Black arcs denote the percentage of all multinucleated cells (to compare with panel A). Results are mean \pm SE as percentage for three independent experiments (total number of nuclei; $n \geq 1000$). (V) EFF-1-expressing cells (red) mixed with EFF-1-expressing cells (cyan) resulted in four cell populations: mononucleate (white pie slice, 44 ± 1.5), multinucleate (red, 24 ± 1.3 ; cyan, 21 ± 3.3), and mixed multinucleated (purple, 11 ± 1 ; $n = 1161$). (VI) In the presence of recombinant monomeric EFF-1 ectodomain: mononucleate (white, 65 ± 3), multinucleate (red, 18 ± 3.2 ; cyan, 13 ± 1.8), and mixed (purple, 4 ± 1.2 ; $n = 1323$). (VII) In the presence of recombinant domain III: mononucleate (white, 69 ± 2.4), multinucleate (red, 15 ± 1.4 ; cyan, 13 ± 1.7), and mixed (purple, 3 ± 1.2 ; $n = 1145$). (VIII) BHK cells expressing empty vector transfected with RFPnes or CFPnl: mononucleate (white, 87 ± 3), binucleate (red, 6 ± 0.4 ; cyan blue, 6 ± 2.6), and mixed (purple, 1 ± 0.3 ; $n = 1287$). See [Experimental Procedures](#) for further details. All experiments were compared with WT EFF-1. * $p < 0.05$; ** $p < 0.005$, two-tailed t test in all experiments. Data are presented as means \pm SEM.

(C) Diagrammatic interpretation of the inhibition by blocking formation of a functional EFF-1 trimer. EFF-1 monomers (colored as in [Figure 1](#), but with domain III shaded to indicate that its location in the monomer is currently not known) interact to form a postfusion trimer, which becomes stabilized upon relocation of domain III to the sides, forming a hairpin that brings the TM segments into contact in the postfusion conformation (top row). Addition of the soluble ectodomain (greyed) interferes with fusion because it adds a subunit without TM segment into a mixed trimer (middle row). Addition of soluble domain III blocks hairpin formation, such that the TM segments cannot be brought into contact (bottom row). For simplicity, only the TM segments are drawn and not the membranes that they cross. See also [Figure S4](#).

monomers to form postfusion trimers. These experiments therefore support the notion that trimerization occurs in *trans*, across membranes, during the fusion reaction.

Addition of Soluble Exogenous Domain III Inhibits Syncytia Formation

Working with alphaviruses and flaviviruses, Kielian and co-workers have shown that addition of the soluble, recombinant domain III of the corresponding fusion protein blocks the membrane fusion reaction (Liao and Kielian, 2005; Sánchez-San Martín et al., 2013). Those experiments demonstrated that an intermediate core trimer of extended protomers inserted in the target membrane forms first, and then domain III folds back to adopt the hairpin conformation and brings the TM segment near the fusion loop. The exogenous domain III acts by binding to the trimeric intermediate and blocking hairpin formation. In the case of EFF-1, we found that addition of soluble domain III inhibits fusion to a similar extent as the intact monomeric ectodomain (Figure 5A). To confirm this observation, we also used a more rigorous method to follow merger of cytoplasms, by applying a cell-culture assay developed previously (Avinoam and Podbilewicz, 2011; Hu et al., 2003). To quantify cytoplasmic mixing, we further transfected the stable EFF-1-expressing BHK cell lines with red fluorescent protein fused to a nuclear export signal (RFPnes), which gives red cytoplasms, or cyan fluorescent protein fused to a nuclear localization signal (CFPnl), which gives cyan nuclei. With this assay, content mixing can be followed for a maximum of 50% of the cells, as same-color-tagged cells will also fuse. In total, for WT EFF-1, we observed that 56% of the cells became multinucleated, with 11% bicolored (i.e., with cyan nuclei in red cytoplasm) and 45% single colored (Figure 5B). This result indicates that same-colored cells had more chance to be in front of each other than different-colored cells, likely because of in-homogeneous mixing. The negative control containing only vector and the RFPnes or CFPnl (Figure 5B, panel IV) showed about 13% binucleate cells, with 1% bicolored, providing the background level of non-EFF-1-mediated fusion—taking into account that same-colored cells may also include dividing cells and/or aborted cytokinesis (Figure 5B, panel VIII) (Podbilewicz et al., 2006). Importantly, we found that content mixing (purple pie slice) was reduced in the cells supplemented with soluble EFF-1 domain III or purified monomeric EFF-1 ectodomain by about a factor of 3 compared to control cells (Figure 5B, panels V–VII), whereas the total multinucleation (sum of the three colored pie slices) is reduced by approximately a factor of 2, matching the results displayed in Figure 5A. Thus, EFF-1-mediated content mixing and syncytia formation can be blocked by monomeric EFF-1 ectodomains and also by soluble domain III, suggesting that cellular and viral class II proteins share a similar fusogenic conformational change (Figure 5C).

EFF-1 Trimerization across Cells Drives Cell-Cell Fusion

The content-mixing results further support the notion that EFF-1 trimerization is required for EFF-1-driven fusion. Furthermore, they constitute evidence that EFF-1 domain III acts in the same way as domain III of the viral class II fusion proteins, for which a block in hairpin formation was demonstrated. Because the binding site for domain III is shared by two adjacent protomers

in the trimer (Figure 3A), these experiments also indicate that formation of an extended intermediate, parallel trimer takes place first, prior to domain III folding back to occupy its postfusion location, as diagrammed in Figure 5C. EFF-1 is therefore not only a structural homolog of class II viral fusion proteins, but it also undergoes trimerization and hairpin formation during the membrane fusion process.

Two important features of EFF-1, however, differentiate it from the viral proteins: the requirement for its presence in both cells to be fused, and the fact that the *cd* loop has a sequence incompatible with membrane insertion. A further element of EFF-1 provided by the structure is that in the postfusion form, the C-terminal ends of the stem of the three subunits converge at the very tip of the molecule, suggesting that the TM segments enter the fused membrane together. The above observations therefore suggest a mechanism for fusion that maintains trimerization and hairpin formation as observed for the viral proteins. The absence of membrane insertion, on the other hand, is most likely related to the fact that trimerization must involve protomers anchored into the two opposing membranes. This is also the case for the SNAREs, which do not insert a fusion loop into the target membrane but cross-oligomerize instead, zipper up the TM segments initially anchored in the two membranes (Stein et al., 2009). The ensemble of the results suggest a mechanism in which the body of the EFF-1 trimer would serve as a scaffold for zipper up the stems, bringing the TM segments into close proximity such that they can continue zipper within the fusing membranes, as diagrammed in Figure 6. The difference with the SNAREs' mechanism is that the same EFF-1 protein is present on the two membranes, albeit with an asymmetry introduced by the fact that the final oligomer is a trimer.

Putative AFF-1/EFF-1 Heterotrimerization

For the above model to apply, it should also account for heterotypic fusion between AFF-1 pseudotyped rhabdoviral particles and EFF-1-expressing cells (Avinoam et al., 2011). Homology modeling of AFF-1 based on the crystal structure of EFF-1 revealed that although the amino acid sequence identity is only 23% (Figure S4), the conserved residues cluster mostly at the trimer interface, compatible with heterotrimerization. The observed plasticity of the trimer interface, as found in the case of the trimerization mutants, is also in line with the protein displaying enough malleability to adapt to EFF-1/AFF-1 heterotrimerization. A further point is the striking conservation of the TM region (Figure S4), which extends to all FF proteins identified to date, and which is also in line with a putative TM zipper during heterotypic fusion mediated by two different FF proteins. The regions where EFF-1 and AFF-1 are most different correspond to the tip of domain II and the MPR, suggesting that heterotypic interactions between these two segments are unlikely. This observation therefore strongly suggests that in the heterotrimer, the MPR is most likely to make homotypic interaction with domain II of the same subunit, implying an intrasubunit stem-domain III connectivity as drawn in Figure 1A.

Do FF Proteins Have a Viral Origin?

Although the structural comparisons reveal that EFF-1 is clearly homologous to the viral class II proteins, it is not possible to

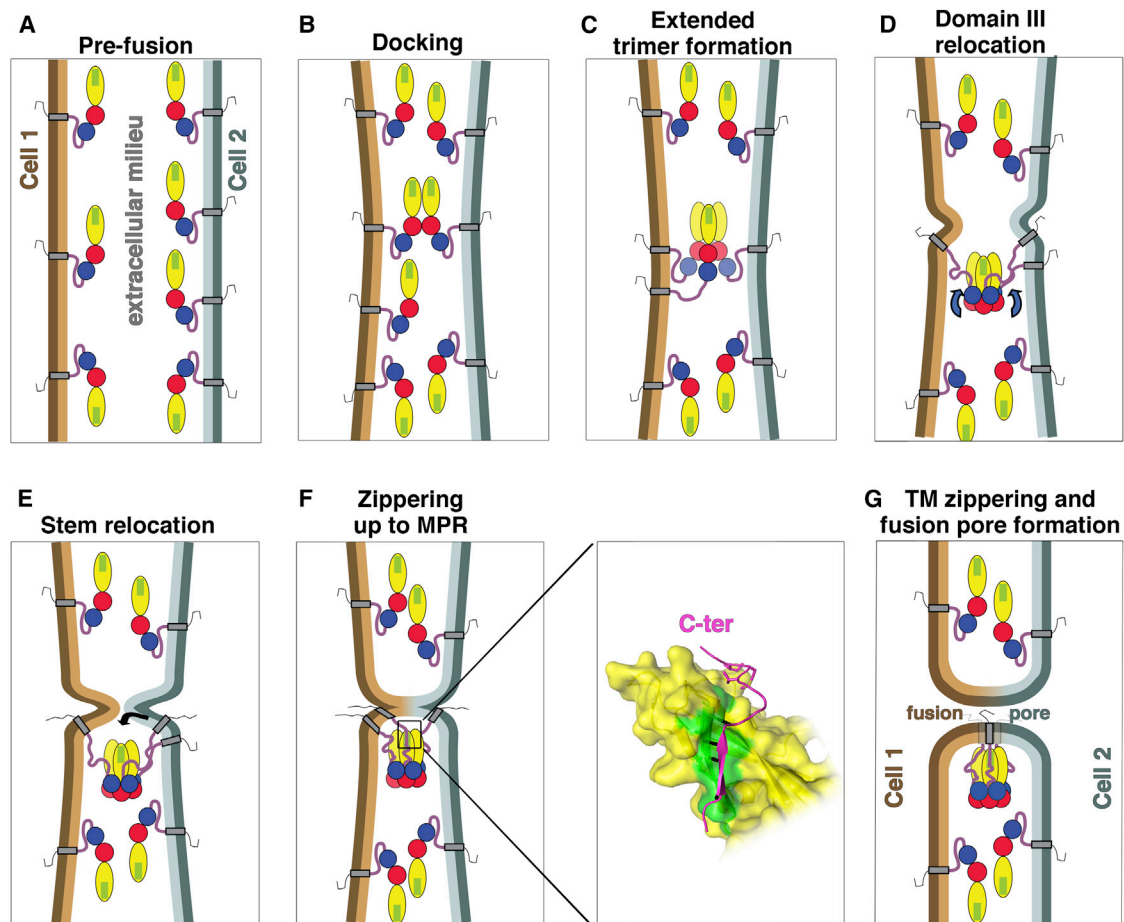


Figure 6. Model for Homotypic EFF-1-Mediated Cell-Cell Fusion

In each panel, the membranes of two cells are represented at either side, with the intercellular space in between; inner and outer leaflets of the plasma membranes are differentiated in dark and pale colors, respectively. EFF-1 is drawn highlighting its domain organization in colors as in Figure 1; the organization of the prefusion form is hypothesized by analogy to the viral counterparts. In domain II (yellow), the green patch represents the region where β strand n and the MPR (magenta) interact to bring the TM segments into contact.

(A) EFF-1 prefusion monomers cluster at the surface of adjacent cells.

(B) Fluctuations at the cell surface result in parallel EFF-1 interactions across cells.

(C) A third monomer, which can come from either cell, adds on to make an intermediate, extended trimer.

(D) Domains III find their binding sites (blue arrows) in between subunits of the extended trimer (see Figure 3A). This reverses the direction of the polypeptide chain, redirecting the stem toward the cd loop region, while simultaneously pulling the two membranes toward each other. At this stage, addition of an exogenous recombinant domain III can block the fusion process, as suggested in Figure 5.

(E) The C-terminal ends of the stems are then in position to interact with the tips of domains II in the trimer.

(F) Positioning the three stems of the trimer into place will bring the N-terminal part of the TM segments into interaction while still within their respective membranes.

(G) We postulate that the TM segments then zipper together, fusing the two membranes, as was postulated for the SNAREs, to complete the fusion process. Bystander, monomeric EFF-1 proteins are drawn in all panels to indicate that only a subset of the proteins may be involved in the fusion process.

See also Figure S1.

assess whether it originally was viral or cellular. Nevertheless, the fact that EFF-1 adopts a hairpin conformation in the postfusion form is more likely to be a remnant of an ancient viral-type membrane-fusion activity. Also, trimerization is not the most straightforward option for an oligomer formed from subunits originally present in two cells. This suggests that trans-trimerization may be a cellular adaptation of a protein that already induced membrane fusion by trimerization with concomitant hairpin formation. It is worth noting that unlike mammalian retroviruses,

the *C. elegans* retroviruses that have been identified have an envelope protein homologous to the phlebovirus fusion protein (Frame et al., 2001; Malik et al., 2000), which also belongs to class II (Dessau and Modis, 2013). It is thus possible that, as in placenta formation, the FF proteins may have a retroviral origin. In contrast to the syncytins, however, which have retained a fusion peptide and function as bona fide viral fusion proteins, the FF proteins have evolved a distinct trans-trimerization fusion mechanism, which also confers them with fusion specificity.

Concluding Remarks

The structural data reported here for a genuine cell-cell fusion protein unambiguously demonstrate an evolutionary link with viral fusion proteins. They constitute a further illustration of the extensive genetic exchanges between viruses and cells throughout evolution and of the striking adaptation of a protein to maintain the same function while adopting an altered mode of action. These data now open the way to a full mechanistic characterization of membrane fusion induced by FF proteins. Our results thus raise a number of new questions, such as the organization of the TM segments in the postfusion trimer, the structure of the prefusion form and its organization on membranes, and how the proposed trans-trimerization fusogenic process is triggered. Finally, these findings provide additional elements that can help in identifying an as yet elusive sequence signature for the class II protein fold and will therefore stimulate the use of structural homology searches to discover unidentified fusion protein homologs in other eukaryotic organisms, for instance, in mammals.

EXPERIMENTAL PROCEDURES

Expression and Purification of EFF-1 Ectodomains

Full-length and truncated versions of the WT and mutant EFF-1 ectodomains were cloned into a modified *Drosophila* S2 expression vector described previously, and transfection was performed as reported earlier (Krey et al., 2010). For large-scale production, cells were induced with 4 μ M CdCl₂ at a density of approximately 7×10^6 cells per milliliter for 8 days and pelleted, and the EFF-1 ectodomains were purified by affinity chromatography from the supernatant using a StrepTactin Superflow column followed by SEC using a Superdex200 column. Pure trimer was concentrated to approximately 11 mg/ml and enzymatically deglycosylated using Endoglycosidase H following the manufacturer's instructions.

Crystallization and Structure Determination

Briefly, we first obtained cubic crystals (space group I2₁3) with one protomer in the asymmetric unit diffracting to ~ 3 Å resolution from a construct spanning the full-length EFF-1 ectodomain (residues 23–561). Using the data from a Gold derivative and the multiple isomorphous replacement and anomalous scattering method, we calculated an electron density map good enough to build a polyalanine model accounting for $\sim 55\%$ of the C α atoms, including a domain exhibiting an immunoglobulin superfamily fold. The initial map further allowed introduction of the amino acid sequence for this domain (aa 409–509), which was compatible with domain III in the structure of viral class II postfusion trimers. Based on this initial model, we truncated the construct at the C terminus of this domain, which crystallized in two different crystal forms, monoclinic (space group C2) and hexagonal (space group P6₃), the first containing a trimer and the second a single protomer in the asymmetric unit and diffracting to 2.7 Å and 2.6 Å resolution, respectively (Table S1). A further selenomethionine (SeMet) derivative crystal of the C2 form, together with 5-fold real-space averaging of the electron density maps of the three crystal forms, resulted in a very clear electron density map, which allowed tracing the whole ectodomain but for a few breaks. The final truncated model was refined to 2.6 Å resolution in the hexagonal form, and the full-length ectodomain to 3 Å in the cubic crystal form.

SEC-MALLS

Purified EFF-1 ectodomains at the indicated concentrations were subjected to SEC using a Superdex 200 column. Online multiangle laser light scattering (MALLS) detection was performed using a laser emitting at 690 nm. Data were analyzed, and weight-averaged molecular masses (Mw) and mass distributions (polydispersity) for each sample were calculated using the ASTRA software (Wyatt Technology, Santa Barbara, CA, USA).

Cell-Cell Fusion Assays with Transiently Expressed EFF-1 and Mutants

BHK cells at 70% confluence were cotransfected with EFF-1 or EFF-1 mutants. As controls, we transfected the empty vector together with the RFPnes construct (lane "vector" in Figure 4C) or the RFPnes construct alone (1 μ g) ("RFPnes only" lane). Cells were fixed 24 hr post-transfection. To determine multinucleation by immunofluorescence, EFF-1 expression was determined using an anti-V5 monoclonal antibody (Invitrogen), and the nuclei stained with DAPI. The fusion indices were defined as the ratio between the total number of nuclei in fused (i.e., multinucleated) cells and total number of nuclei in expressing cells that coexpress RFPnes and that were in contact (Podbilewicz et al., 2006). The fusion indexes are presented as percentage means \pm SEM of three independent experiments ($n_{\text{(nuclei number)}} \geq 1000$ for each experiment and condition). A two-tailed unpaired t test was used to determine significant differences between WT and mutant EFF-1.

Cell Fusion Assay with Stable EFF-1 BHK Transfectants under an Inducible Promoter to Measure Content Mixing

EFF-1 fused to mCherry fluorescent protein was cloned into the pGene vector for inducible expression. Stable BHK cells inducibly expressing EFF-1-mCherry (BHK-EFF-1mCherry) were generated according to the manufacturer's instructions. BHK-EFF-1mCherry cells were transiently transfected with pCFPns or pRFPnes, driving the expression of either a nuclear or a cytoplasmic fluorescent marker. Equal numbers of BHK cells expressing EFF-1-mCherry under an inducible promoter and transiently expressing RFPnes or CFPns were mixed 18 hr after transfection and induced 4 hr later in the absence or presence of ectopic EFF-1 domain III, monomeric or trimeric ectodomain at 200 μ M. Eighteen hours after induction, the cells were fixed and DAPI stained, and the nuclei counted. The percentage of cytoplasmic content mixing was defined as the ratio between the number of nuclei (CFP) in RFP mCherry-expressing cells and the total number of counted nuclei. Three independent experiments were performed as duplicates, and the mean values of the three experiments are shown with SEM. Statistical differences were determined as described above.

Biotinylation of EFF-1 Expressed on BHK Cell Surface

BHK cells were transfected with the desired vector (described in the legend to Figure 4C) followed by cell-surface labeling with Sulfo-NHS-biotin at 0°C (to prevent endocytosis). Cells were washed, resuspended in lysis buffer, and kept on ice. Biotinylated proteins were precipitated using neutravidin agarose resin, and the precipitate was washed extensively. The precipitated complex was mixed with reducing SDS-PAGE loading buffer and incubated at 95°C for 5 min. After pelleting of the neutravidin agarose beads, the supernatant was analyzed by SDS-PAGE. The proteins were analyzed by western blot with an anti-V5 antibody for EFF-1::V5 detection and a monoclonal anti-human actin for detection of actin used as loading control.

ACCESSION NUMBERS

The atomic coordinates and structure factors of three structures have been deposited in the Protein Data Bank, www.pdb.org, with accession numbers 4OJC, 4OJD, and 4OJE.

SUPPLEMENTAL INFORMATION

Supplemental Information includes Extended Experimental Procedures, six figures, and three tables and can be found with this article online at <http://dx.doi.org/10.1016/j.cell.2014.02.020>.

AUTHOR CONTRIBUTIONS

B.P. and F.A.R. conceived the experiments. J.P.-V. made the constructs and crystallized and optimized the crystals for diffraction. T.K. made WT and mutant C-terminally truncated constructs and determined the EFF-1 X-ray structure. C.V. performed surface biotinylation of WT and EFF-1 proteins, C.V. and O.A. conducted cell fusion assays and fluorescence microscopy, O.A. and

H.R.-B. made constructs of WT and mutant EFF-1, A.H. devised a protocol for crystal cryoprotection, and M.J. performed the MALLS analysis. T.K., B.P., and F.A.R. wrote the manuscript with input from all the other authors.

ACKNOWLEDGMENTS

F.A.R. was funded by the French "Agence Nationale pour la Recherche" grant ANR-2010-BLAN-1211 01 and by Institut Pasteur, CNRS, and Merck-Serono. B.P. was funded by the ERC Advanced grant 268843 and the Israel Science Foundation (ISF grants 1542/07 and 826/08). B.P. was a Grass fellow at Radcliffe Institute for Advanced Study, Harvard University. We thank Patrick England, Bertrand Raynal, and Patrick Weber of the Pasteur Proteopole for technical help; the staff of synchrotron beamlines PX-I at the Swiss Light Source, Proxima-1 at SOLEIL, and ID23-1 at the European Synchrotron Radiation Facility for help during data collection; Clemens Vornrhein and Gerard Bricogne from Global Phasing Ltd. for methodological concepts; Tom Rapoport and his lab for discussions and for hosting B.P. at Harvard Medical School; and Jorge Verdin Ramos from Technion and the members of the Rey and Podbilewicz labs for discussions.

Received: July 1, 2013

Revised: January 1, 2014

Accepted: February 6, 2014

Published: April 10, 2014

REFERENCES

- Aguilar, P.S., Baylies, M.K., Fleissner, A., Helming, L., Inoue, N., Podbilewicz, B., Wang, H., and Wong, M. (2013). Genetic basis of cell-cell fusion mechanisms. *Trends Genet.* **29**, 427–437.
- Avinoam, O., Fridman, K., Valansi, C., Abutbul, I., Zeev-Ben-Mordehai, T., Maurer, U.E., Sapir, A., Danino, D., Grünwald, K., White, J.M., and Podbilewicz, B. (2011). Conserved eukaryotic fusogens can fuse viral envelopes to cells. *Science* **332**, 589–592.
- Avinoam, O., and Podbilewicz, B. (2011). Eukaryotic cell-cell fusion families. *Curr. Top. Membr.* **68**, 209–234.
- Bian, X., Klemm, R.W., Liu, T.Y., Zhang, M., Sun, S., Sui, X., Liu, X., Rapoport, T.A., and Hu, J. (2011). Structures of the atlastin GTPase provide insight into homotypic fusion of endoplasmic reticulum membranes. *Proc. Natl. Acad. Sci. USA* **108**, 3976–3981.
- Blond, J.L., Besème, F., Duret, L., Bouton, O., Bedin, F., Perron, H., Mandrand, B., and Mallet, F. (1999). Molecular characterization and placental expression of HERV-W, a new human endogenous retrovirus family. *J. Virol.* **73**, 1175–1185.
- Blond, J.L., Lavillette, D., Cheynet, V., Bouton, O., Oriol, G., Chapel-Fernandes, S., Mandrand, B., Mallet, F., and Cosset, F.L. (2000). An envelope glycoprotein of the human endogenous retrovirus HERV-W is expressed in the human placenta and fuses cells expressing the type D mammalian retrovirus receptor. *J. Virol.* **74**, 3321–3329.
- Bressanelli, S., Stiasny, K., Allison, S.L., Stura, E.A., Duquerroy, S., Lescar, J., Heinz, F.X., and Rey, F.A. (2004). Structure of a flavivirus envelope glycoprotein in its low-pH-induced membrane fusion conformation. *EMBO J.* **23**, 728–738.
- Byrnes, L.J., and Sondermann, H. (2011). Structural basis for the nucleotide-dependent dimerization of the large G protein atlastin-1/SPG3A. *Proc. Natl. Acad. Sci. USA* **108**, 2216–2221.
- del Campo, J.J., Opoku-Serebuoh, E., Isaacson, A.B., Scranton, V.L., Tucker, M., Han, M., and Mohler, W.A. (2005). Fusogenic activity of EFF-1 is regulated via dynamic localization in fusing somatic cells of *C. elegans*. *Curr. Biol.* **15**, 413–423.
- Dessau, M., and Modis, Y. (2013). Crystal structure of glycoprotein C from Rift Valley fever virus. *Proc. Natl. Acad. Sci. USA* **110**, 1696–1701.
- DuBois, R.M., Vaney, M.-C., Tortorici, M.A., Kurdi, R.A., Barba-Spaeth, G., Krey, T., and Rey, F.A. (2013). Functional and evolutionary insight from the crystal structure of rubella virus protein E1. *Nature* **493**, 552–556.
- Frame, I.G., Cutfield, J.F., and Poulter, R.T. (2001). New BEL-like LTR-retrotransposons in *Fugu rubripes*, *Caenorhabditis elegans*, and *Drosophila melanogaster*. *Gene* **263**, 219–230.
- Gibbons, D.L., Vaney, M.C., Roussel, A., Vigouroux, A., Reilly, B., Lepault, J., Kielian, M., and Rey, F.A. (2004). Conformational change and protein-protein interactions of the fusion protein of Semliki Forest virus. *Nature* **427**, 320–325.
- Harrison, S.C. (2008). Viral membrane fusion. *Nat. Struct. Mol. Biol.* **15**, 690–698.
- Holm, L., and Park, J. (2000). DaliLite workbench for protein structure comparison. *Bioinformatics* **16**, 566–567.
- Hu, C., Ahmed, M., Melia, T.J., Sollner, T.H., Mayer, T., and Rothman, J.E. (2003). Fusion of cells by flipped SNAREs. *Science* **300**, 1745–1749.
- Jahn, R., and Scheller, R.H. (2006). SNAREs—engines for membrane fusion. *Nat. Rev. Mol. Cell Biol.* **7**, 631–643.
- Kielian, M., and Rey, F.A. (2006). Virus membrane-fusion proteins: more than one way to make a hairpin. *Nat. Rev. Microbiol.* **4**, 67–76.
- Klein, D.E., Choi, J.L., and Harrison, S.C. (2013). Structure of a dengue virus envelope protein late-stage fusion intermediate. *J. Virol.* **87**, 2287–2293.
- Kozlov, M.M., McMahon, H.T., and Chernomordik, L.V. (2010). Protein-driven membrane stresses in fusion and fission. *Trends Biochem. Sci.* **35**, 699–706.
- Krey, T., d'Alayer, J., Kikuti, C.M., Saulnier, A., Damier-Piolle, L., Petitpas, I., Johansson, D.X., Tawar, R.G., Baron, B., Robert, B., et al. (2010). The disulfide bonds in glycoprotein E2 of hepatitis C virus reveal the tertiary organization of the molecule. *PLoS Pathog.* **6**, e1000762.
- Kuhn, R.J., Zhang, W., Rossmann, M.G., Pletnev, S.V., Corver, J., Lenches, E., Jones, C.T., Mukhopadhyay, S., Chipman, P.R., Strauss, E.G., et al. (2002). Structure of dengue virus: implications for flavivirus organization, maturation, and fusion. *Cell* **108**, 717–725.
- Lescar, J., Roussel, A., Wien, M.W., Navaza, J., Fuller, S.D., Wengler, G., Wengler, G., and Rey, F.A. (2001). The Fusion glycoprotein shell of Semliki Forest virus: an icosahedral assembly primed for fusogenic activation at endosomal pH. *Cell* **105**, 137–148.
- Liao, M., and Kielian, M. (2005). Domain III from class II fusion proteins functions as a dominant-negative inhibitor of virus membrane fusion. *J. Cell Biol.* **171**, 111–120.
- Luca, V.C., Nelson, C.A., and Fremont, D.H. (2013). Structure of the St. Louis encephalitis virus postfusion envelope trimer. *J. Virol.* **87**, 818–828.
- Malik, H.S., Henikoff, S., and Eickbush, T.H. (2000). Poised for contagion: evolutionary origins of the infectious abilities of invertebrate retroviruses. *Genome Res.* **10**, 1307–1318.
- Mi, S., Lee, X., Li, X., Veldman, G.M., Finnerty, H., Racie, L., LaVallie, E., Tang, X.Y., Edouard, P., Howes, S., et al. (2000). Syncytin is a captive retroviral envelope protein involved in human placental morphogenesis. *Nature* **403**, 785–789.
- Modis, Y., Ogata, S., Clements, D., and Harrison, S.C. (2004). Structure of the dengue virus envelope protein after membrane fusion. *Nature* **427**, 313–319.
- Mohler, W.A., Shemer, G., del Campo, J.J., Valansi, C., Opoku-Serebuoh, E., Scranton, V., Assaf, N., White, J.G., and Podbilewicz, B. (2002). The type I membrane protein EFF-1 is essential for developmental cell fusion. *Dev. Cell* **2**, 355–362.
- Moss, T.J., Daga, A., and McNew, J.A. (2011). Fusing a lasting relationship between ER tubules. *Trends Cell Biol.* **21**, 416–423.
- Nayak, V., Dessau, M., Kucera, K., Anthony, K., Ledizet, M., and Modis, Y. (2009). Crystal structure of dengue virus type 1 envelope protein in the postfusion conformation and its implications for membrane fusion. *J. Virol.* **83**, 4338–4344.
- Podbilewicz, B., Leikina, E., Sapir, A., Valansi, C., Suissa, M., Shemer, G., and Chernomordik, L.V. (2006). The *C. elegans* developmental fusogen EFF-1 mediates homotypic fusion in heterologous cells and in vivo. *Dev. Cell* **11**, 471–481.

- Rey, F.A., Heinz, F.X., Mandl, C., Kunz, C., and Harrison, S.C. (1995). The envelope glycoprotein from tick-borne encephalitis virus at 2 Å resolution. *Nature* 375, 291–298.
- Sánchez-San Martín, C., Nanda, S., Zheng, Y., Fields, W., and Kielian, M. (2013). Cross-inhibition of chikungunya virus fusion and infection by alphavirus E1 domain III proteins. *J. Virol.* 87, 7680–7687.
- Sapir, A., Choi, J., Leikina, E., Avinoam, O., Valansi, C., Chernomordik, L.V., Newman, A.P., and Podbilewicz, B. (2007). AFF-1, a FOS-1-regulated fusogen, mediates fusion of the anchor cell in *C. elegans*. *Dev. Cell* 12, 683–698.
- Sapir, A., Avinoam, O., Podbilewicz, B., and Chernomordik, L.V. (2008). Viral and developmental cell fusion mechanisms: conservation and divergence. *Dev. Cell* 14, 11–21.
- Shemer, G., Suissa, M., Kolotuev, I., Nguyen, K.C., Hall, D.H., and Podbilewicz, B. (2004). EFF-1 is sufficient to initiate and execute tissue-specific cell fusion in *C. elegans*. *Curr. Biol.* 14, 1587–1591.
- Shilagardi, K., Li, S., Luo, F., Marikar, F., Duan, R., Jin, P., Kim, J.H., Murnen, K., and Chen, E.H. (2013). Actin-propelled invasive membrane protrusions promote fusogenic protein engagement during cell-cell fusion. *Science* 340, 359–363.
- Stein, A., Weber, G., Wahl, M.C., and Jahn, R. (2009). Helical extension of the neuronal SNARE complex into the membrane. *Nature* 460, 525–528.
- Südhof, T.C., and Rothman, J.E. (2009). Membrane fusion: grappling with SNARE and SM proteins. *Science* 323, 474–477.
- Sutton, R.B., Fasshauer, D., Jahn, R., and Brunger, A.T. (1998). Crystal structure of a SNARE complex involved in synaptic exocytosis at 2.4 Å resolution. *Nature* 395, 347–353.
- Wickner, W., and Schekman, R. (2008). Membrane fusion. *Nat. Struct. Mol. Biol.* 15, 658–664.